

Amplification of Acoustic Evanescent Waves Using Metamaterial Slabs

Choon Mahn Park,¹ Jong Jin Park,² Seung Hwan Lee,² Yong Mun Seo,³ Chul Koo Kim,² and Sam H. Lee^{2,*}

¹*AEE Center, Anyang University, Anyang 430-714, Korea*

²*Institute of Physics and Applied Physics, Yonsei University, Seoul 120-749, Korea*

³*Department of Physics, Myongji University, Yongin 449-728, Korea*

(Received 31 May 2011; published 1 November 2011)

We amplified acoustic evanescent waves using metamaterial slabs with a negative effective density. For the amplifying effect of the slab to overcome the dissipation, it is necessary that the imaginary part of the effective density is much smaller than the real part, a condition not satisfied so far. We report the construction of membrane-based two-dimensional negative-density metamaterials which exhibited remarkably small dissipation. Using a slab of this metamaterial we realized a 17-fold net amplitude gain at a remote distance from the evanescent wave source. Potential applications include acoustic superlensing.

DOI: 10.1103/PhysRevLett.107.194301

PACS numbers: 43.90.+v, 43.40.+s

The amplification of electromagnetic evanescent waves was provided by slabs of negative-permittivity materials and eventually led to superlensing [1–11]. For acoustic waves, Ambati *et al.* theoretically demonstrated that a slab of metamaterial with a negative density (ρ -NG) can amplify evanescent waves [12]. The amplification of acoustic evanescent waves using metamaterials, however, has not been realized so far due to the dissipation problem.

Previously reported two- or more-dimensional ρ -NG materials consisted of fluid with embedded floating double resonators, which consist of inner and outer mass coupled by springs [Fig. 1(a)] [13–15]. When the outer mass is subject to a sinusoidal driving force, the inner and the outer mass move 180° out of phase in a certain frequency range. In this case, even though the acceleration of the center of mass of the total double resonator system is along the direction of the applied force, the outer shell accelerates in the opposite direction, making the effective mass negative. However, the motion of the filling fluid outside the double resonator is along the inner mass, opposite to the motion of the outer shell. Since the outer shell is in direct contact with the fluid, this opposite motion inevitably results in a heavy velocity shear in the fluid and a considerable dissipation.

To eliminate this loss, it is necessary to find a method to make the fluid move together with the double resonator. In this Letter, we present the idea of using membranes as shown in Fig. 1(b). Membranes block the fluid and, thus, make the average velocity of the fluid the same as that of the outer shell. This structure has an additional advantage that the membrane also functions as a sustaining structure of the double resonator in place. Some tension is needed for the membrane to be able to hold the fluid to move with the outer shell. This tension, however, adds an action that was absent in the original double resonator system: The membrane gives an extra force on the outer shell when it is displaced from the original place. Even though this additional force alters the dispersion relation of the effective

density, it does not change the occurrence of the negative density. Since all we need is a negative density with small dissipation, this change is acceptable.

Remarkably, it turns out that the restoring force term from the stretched membrane alone can generate negative density [16]. In other words, the membrane in the structure

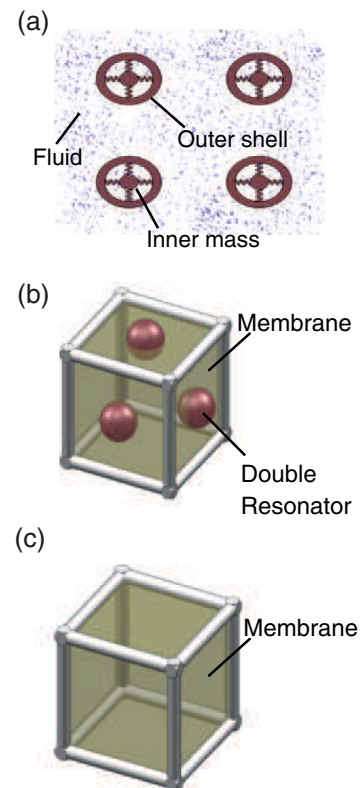


FIG. 1 (color online). Progress of the idea for a negative-density metamaterial with small dissipation. (a) Lattice of double resonators embedded in a fluid. (b) Membranes are installed to make the fluid move together with the double resonator. (c) Structure with the membranes that generates a negative density.

shown in Fig. 1(b), introduced to block the fluid, makes the negative-density-generating action of the double resonator redundant. That is, we can remove the double resonator in the structure 1(b) and still get the negative density. When the double resonators in the structure 1(b) are removed, it is rendered to the structure shown in Fig. 1(c), which consists only of the stretched membranes. It is the structure 1(c) we fabricated for the amplification of acoustic evanescent waves, even though the structure 1(b) would have also given successful results.

We constructed 2D ρ -NG acoustic metamaterial as shown in Fig. 2. The unit cell is a square-shaped compartment of dimension $43 \text{ mm} \times 43 \text{ mm}$ consisting of 2 mm thick plastic walls with round openings. These openings are of 15 mm radius and accommodate 0.01 mm thick low density polyethylene film stretched to 65 N/m tension and attached airtight to the rims. The top and bottom of each compartment are covered with 5 mm thick plastic plates: The whole assembly of 128 compartments was built on a large bottom plate as shown in Fig. 2(a), and then a large plate was placed on top. The resulting air-filled metamaterial structure is a two-dimensional version of the previously reported 1D ρ -NG structure based on thin tight membranes [16–18]. The top and bottom plates were larger than the metamaterial slab and extended out to both sides

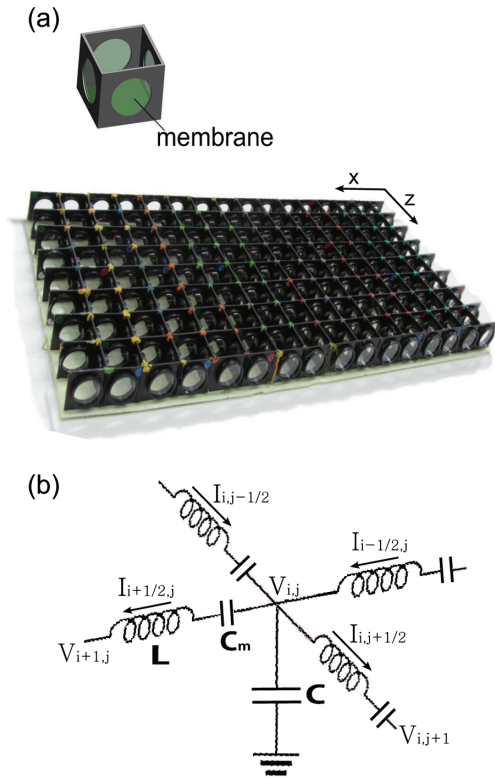


FIG. 2 (color online). (a) The unit cell consists of four identical windows of thin elastic membranes. Photo of two-dimensional ρ -NG acoustic metamaterial with the top cover removed. (b) The equivalent circuit of the unit cell.

of the metamaterial. Beyond the left and the right ends of the metamaterial, there was nothing but air between the two plates. Therefore, two air-metamaterial interfaces were formed. The ρ -NG metamaterial slab shown in Fig. 2(a) turned out to have extremely small loss and amplified acoustic evanescent waves.

The effective density of the present system, which is clearly isotropic due to the square lattice structure, can be obtained by considering plane waves propagating along the $[1, 0]$ direction, which we designate as the x direction. Since the particle velocity has only an x component, the windows oriented parallel to the x direction do not move at all. This structure, then, cannot be distinguished from the previously reported 1D ρ -NG structure exhibiting an effective density and modulus given by [16–18],

$$\rho_{\text{eff}} = \rho' \left(1 - \frac{\omega_c^2}{\omega^2} \right), \quad B_{\text{eff}} = B_a, \quad (1)$$

where ρ' and B_a are the averaged mass density of air and membrane and the modulus of air, respectively.

Now, we shall use the transmission line model [19–22] to analytically demonstrate that the effective parameters of our system are indeed as described by Eq. (1). Our acoustic system can be represented by the two-dimensional array of the unit circuit structure shown in Fig. 2(b). The voltage V_{ij} at the cross junction above the shunt capacitor C corresponds to the pressure in the unit cell at the i th row (along the x axis) and j th column (along the z axis). Also, the current $I_{i+1/2,j}$, for example, represents the volume flow of air from the cell (i, j) to the cell $(i + 1, j)$. Shunt capacitance C and series inductance L are proportional to the compressibility ($C \leftrightarrow \Omega/B_a$) and mass ($L \leftrightarrow M/S^2$) of the system, where Ω , S , B_a , and M are the volume, cross sectional area, bulk modulus, and mass of the unit cell, respectively [21]. In this analysis, membranes can be considered as series capacitors C_m in the circuit [19]. The currents are related to the voltages according to Kirchoff's laws [22]:

$$\begin{aligned} V_{ij} - V_{i,j+1} &= L \frac{d}{dt} I_{i,j+1/2} + \frac{1}{C_m} \int I_{i,j+1/2} dt, \\ V_{ij} - V_{i+1,j} &= L \frac{d}{dt} I_{i+1/2,j} + \frac{1}{C_m} \int I_{i+1/2,j} dt, \\ I_{i,j-1/2} + I_{i-1/2,j} - I_{i+1/2,j} - I_{i,j+1/2} &= C \frac{dV_{ij}}{dt}. \end{aligned} \quad (2)$$

Since the lattice constant a is much smaller than the wavelength λ , the discrete nature of the structure can be homogenized, and the circuit array can be regarded as a continuous 2D transmission line with the voltage distribution $V(x, z)$ and the current density $\vec{J}(x, z)$. The current density in 2D space has the dimension of A/m. By using harmonic expressions, Eq. (2) becomes

$$\nabla V = \left(i\omega L' + \frac{1}{i\omega C'_m} \right) \vec{J} = i\omega L'_{\text{eff}} \vec{J}, \quad (3)$$

$$\nabla \cdot \vec{J} = i\omega C' V = i\omega C'_{\text{eff}} V,$$

where L' , C'_m , and C' are “per-unit-area” quantities of the series inductance, the series capacitance, and the shunt capacitance, respectively. It can be shown that, for a square lattice, $L' = L$, $C'_m = C_m$, and $C' = C/a^2$. From Eq. (3), we obtain

$$L'_{\text{eff}} = L' \left(1 - \frac{\omega_c^2}{\omega^2} \right), \quad C'_{\text{eff}} = C', \quad (4)$$

where $\omega_c = \sqrt{1/(L'C'_m)}$.

The physics in the circuit maps exactly to that in the acoustic metamaterial, and there are one-to-one correspondences for all quantities. The constitutive parameters L'_{eff} for the circuit corresponds to the effective mass density of the system and the C'_{eff} to the bulk modulus. From Eq. (4), it is clear that $\rho_{\text{eff}} = \rho' \sqrt{1 - \omega_c^2/\omega^2}$ and that the effective bulk modulus B_{eff} remains the same as that of air B_a , $B_{\text{eff}} = B_a$, because the per-unit-area shunt capacitance C' is proportional to the compressibility of air. Therefore, from the analysis using circuit representation, we theoretically proved that the effective density and modulus of our 2D ρ -NG system are as given by Eq. (1).

We experimentally demonstrate net amplification of acoustic evanescent waves provided by this metamaterial slab as shown in Fig. 3. An acoustic evanescent wave was generated by using an array of four identical speakers: Each speaker is represented by the dots marked with “+” or “−” in Fig. 3. The four speakers are connected to a 462 Hz signal source, but the leads for those two speakers marked with − are connected in exchanged polarity so that the sound coming from them is 180° out of phase from those marked with +. Since the spacing of the speaker array (23 cm) is shorter than the half wavelength (37 cm), the evanescent waves shown in Fig. 3(a) are generated. It can be seen that there is practically no signal left in the region $z > 0$. The pressure amplitude of the evanescent wave, measured as a function of z at x of a speaker, is shown with solid circles in Fig. 3(a): Rapid decay of the evanescent wave is clear.

Figure 3(b) shows the experimental result of the pressure profile when the metamaterial slab was inserted. The signal in the region $z > 0$ was significantly enhanced and became clearly visible. About 17-fold net amplification was obtained. Square points are the experimental pressure amplitude data along the z direction at x of a speaker. Interestingly, the pressure amplitude was increased on the left side of the slab as well. This indicates that, as pointed out by Ambati *et al.*, a resonance was taking place in the metamaterial slab.

The net amplification is dependent on the dissipation of metamaterial [23]. The dissipation, accounted as the

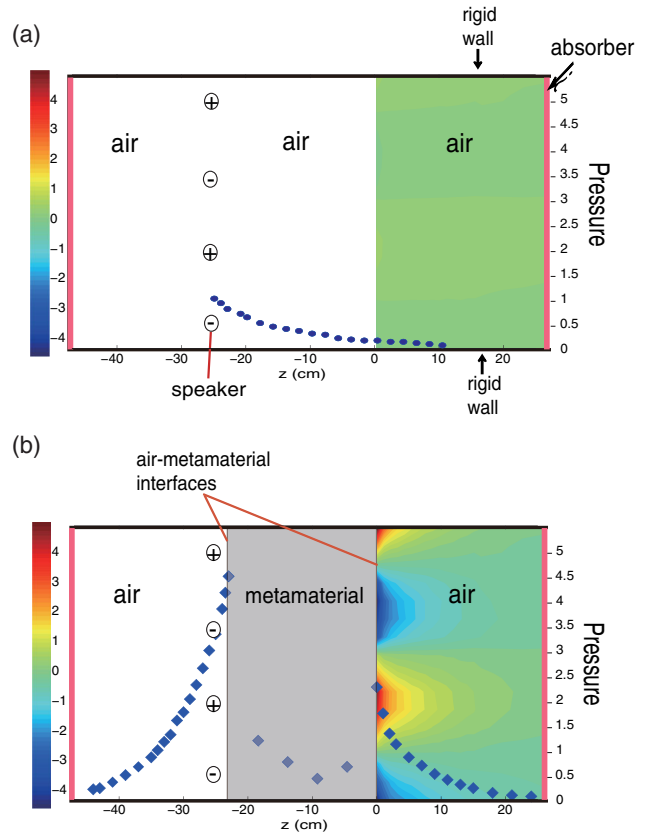


FIG. 3 (color online). Amplification of evanescent wave with wave vector $k = 1.6k_0$ and $f = 462$ Hz. Pressure amplitude was normalized with the amplitude at the source without a metamaterial. Color maps represent the distribution of acoustic pressure. (a) The amplitude of the evanescent pressure field without a metamaterial. (b) The amplitude of the evanescent pressure field with a metamaterial.

imaginary part of the density, can be calculated from the net amplification and thickness of the slab [8–12]. In our system, the imaginary part was about 4% of the real part of the density. The dissipation is remarkably small because the membranes move together with the fluid.

As surface plasmons are excited on negative-permittivity materials, novel acoustic surface excitations are expected to be excited on a ρ -NG acoustic metamaterial [12]. We observed such surface waves excited by a point source placed at a corner of the metamaterial surface as shown in Fig. 4(a). To make the intensities of the surface waves better detectable, we generated standing waves of the surface waves by making the length of the interface finite. Since the point source has Fourier components for all possible wave vectors, standing waves with the right dispersion for the given frequency were generated. One of the typical standing surface waves is shown in Fig. 4(b): It is an experimentally measured “snapshot” of pressure distribution in the air side at the frequency of 462 Hz. The wavelength of this surface wave was $\lambda_{\text{sp}} = 0.46$ m, which was smaller than the wavelength in air $\lambda_0 = 0.74$ m.

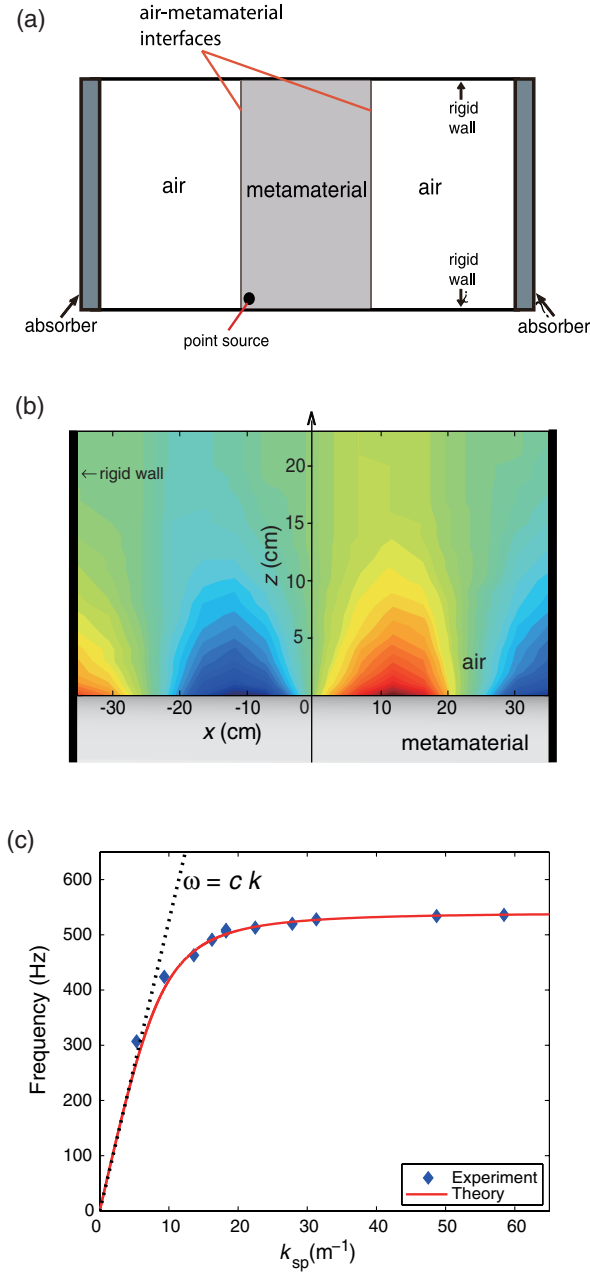


FIG. 4 (color online). (a) Schematic diagram of the experimental setup to measure the dispersion relation of the acoustic surface waves. A point source was used to excite the surface waves. (b) Pressure distribution of the surface wave in the air at $f = 462$ Hz. The interface between the air ($z > 0$) and the metamaterial ($z < 0$) is indicated by the $z = 0$ plane. (c) Theoretical and experimental dispersion relation of the acoustic surface wave. Experimental results agree excellently with the theoretical curve calculated from Eq. (5). The wave vector diverges at the frequency where $\rho_{\text{eff}} = -\rho_a$.

The wave vectors $k_{\text{sp}} = 2\pi/\lambda_{\text{sp}}$ determined for the frequencies that gave standing waves are shown in Fig. 4(c). The dispersion of the surface wave is given by $k_{\text{sp}} = k_0 \sqrt{\rho_{\text{eff}}/(\rho_a + \rho_{\text{eff}})}$ [12], where k_0 is the wave vector in

air. The wave vector of the surface waves is explicitly obtained by using Eq. (1):

$$k_{\text{sp}}(\omega) = k_0 \left[1 + \frac{\rho_a}{\rho'} \left(\frac{\omega^2}{\omega^2 - \omega_c^2} \right) \right]^{-1/2}, \quad (5)$$

where ρ_a is the density of air. The theoretical curve from Eq. (1) agrees excellently with the experimental data, and the dispersion curve has exactly the same shape as that of the plasmon on a metal surface. We observed acoustic surface waves theoretically predicted by Ambati *et al.*, and the wave characteristics are similar to those of the surface plasmons on the metal. The wave vector diverges to infinity at the frequency $\omega_1 = \omega_c \sqrt{\rho'/(\rho' + \rho_a)}$, or $\omega_1 = 0.73$, $\omega_c = 534$ Hz for the present system.

The amplitude ratio of two surface waves on the two air-metamaterial interfaces is sensitively dependent on the thickness and the dissipation of the slab [23]. The dissipation can be calculated from the amplitude ratio of surface excitations on the metamaterial surfaces [8,12]. In our metamaterial, the absolute value of estimated dissipation is $0.07\rho_a \ll |\rho_{\text{eff}}| = 2.10 \text{ kg/m}^3$. Reasons for this small dissipation are as follows: (i) The surface waves were excited at the frequencies below $0.73\omega_c$, and, thus, dissipation related to local resonance was negligible. (ii) In the metamaterial consisting of membranes, the membranes move together with the fluid so that the friction between them is small. The small dissipation allowed us to observe novel surface acoustic waves on the metamaterial in a wide frequency range ($\omega < 0.73\omega_c$) and the amplification of evanescent waves through this surface excitation. Therefore, our work opens the possibility for the realization of acoustic superlensing.

This research was supported by Basic Science Research Program through the National Research Foundation of Korea (NRF) funded by the Ministry of Education, Science and Technology (NRF 2010-0012562).

*samlee@yonsei.ac.kr

- [1] D.R. Smith, *Science* **308**, 502 (2005).
- [2] S. Kawata, Y. Inouye, and P. Verma, *Nat. Photon.* **3**, 388 (2009).
- [3] H. Lee *et al.*, *New J. Phys.* **7**, 255 (2005).
- [4] I.I. Smolyaninov, Y.-J. Hung, and C.C. Davis, *Science* **315**, 1699 (2007).
- [5] M.W. Feise, P.J. Bevelacqua, and J.B. Schneider, *Phys. Rev. B* **66**, 035113 (2002).
- [6] X. Zhang and Z. Liu, *Nature Mater.* **7**, 435 (2008).
- [7] N. Fang *et al.*, *Opt. Express* **11**, 682 (2003).
- [8] J.B. Pendry, *Phys. Rev. Lett.* **85**, 3966 (2000).
- [9] N. Fang *et al.*, *Science* **308**, 534 (2005).
- [10] K.G. Balmain, A.A.E. Lüttgen, and P.C. Kremer, *IEEE Antennas Wireless Propag. Lett.* **1**, 146 (2002).
- [11] J.B. Pendry, A.J. Holden, W.J. Stewart, and I. Youngs, *Phys. Rev. Lett.* **76**, 4773 (1996).

- [12] M. Ambati, N. Fang, C. Sun, and X. Zhang, *Phys. Rev. B* **75**, 195447 (2007).
- [13] Z. Liu *et al.*, *Science* **289**, 1734 (2000).
- [14] H. Larabi, Y. Pennec, B. Djafari-Rouhani, and J. O. Vasseur, *Phys. Rev. E* **75**, 066601 (2007).
- [15] C. Goffaux, J. Sánchez-Dehesa, and P. Lambin, *Phys. Rev. B* **70**, 184302 (2004).
- [16] S. H. Lee, C. M. Park, Y. M. Seo, Z. G. Wang, and C. K. Kim, *Phys. Lett. A* **373**, 4464 (2009).
- [17] S. H. Lee, C. M. Park, Y. M. Seo, Z. G. Wang, and C. K. Kim, *Phys. Rev. Lett.* **104**, 054301 (2010).
- [18] S. H. Lee, C. M. Park, Y. M. Seo, and C. K. Kim, *Phys. Rev. B* **81**, 241102(R) (2010).
- [19] F. Bongard, H. Lissek, and J. R. Mosig, *Phys. Rev. B* **82**, 094306 (2010).
- [20] S. Zhang, C. Xia, and N. Fang, *Phys. Rev. Lett.* **106**, 024301 (2011).
- [21] D. T. Blackstock, *Fundamentals of Physical Acoustics* (Wiley, New York, 2000).
- [22] E. Afshari, H. S. Bhat, A. Hajimiri, and J. E. Marsden, *J. Appl. Phys.* **99**, 054901 (2006).
- [23] X. S. Rao and C. K. Ong, *Phys. Rev. B* **68**, 113103 (2003).